Light wave states in two-dimensional quasiperiodic media

K. Wang*
Laboratoire de Physique des Solides, UMR CNRS, 91405 Orsay, France
(Received 1 December 2005; revised manuscript received 14 February 2006; published 27 June 2006)

We study light wave behavior in two-dimensional quasiperiodic dielectric structures through the approximant ones. We show that, unlike the classic cases, light localization occurs in these structures due to local resonances in regions where scatterers form high-symmetry patterns, without involving any disorder. Moreover, introduction of disorder by structure randomization can lead to more extended states and a strong increase in light propagation.

DOI: 10.1103/PhysRevB.73.235122 PACS number(s): 61.44.Br, 42.25.Bs

Light is known to undergo Anderson localization when propagating through disordered strongly scattering dielectric media,[1,2] due to destructive interference between randomly multiscattered waves. This phenomenon has been intensively studied, motivated both by fundamental interest and important applications in various fields,[2,3] involving random laser and disordered photonic band-gap materials.[4] The localization is suppressed in perfectly ordered dielectric media, such as simple periodic photonic crystals,[5] where light waves are described by extended normal states. In the present work, we study the light wave behavior at the photonic gap edges in two-dimensional (2D) quasiperiodic (QP) and related approximant dielectric structures, based on Maxwell's equations, and compare the results with the classical localization cases. QP structures offer many interests as they differ from both the disordered and simple periodic structures from numerous points of view. Indeed, as compared to the former, they are perfectly ordered and determinist; as compared to the latter, they are aperiodic and characterized by higher degree rotational symmetry (for dimension $D \geq 2$) and richer and more general geometrical configurations. Early studies on light propagation in QP dielectric structures were essentially concentrated on 1D cases, focusing on the structure self-similarity and the lack of periodicity.[6] Interest in localized photonic states arises following the discovery of photonic band-gap materials.[5] It has been shown that local resonant cavities[7] as well as localized states inside the photonic gaps[8] are found in 1D aperiodic sequences. In fact, both of these modes are related to artificially introduced segment defects in the sequence structures. There is also indication that light localization occurs at gap edges in defect-free 1D Fibonacci crystals, where computed field intensity is found critically distributed all over the sample.[9] In the 2D case, QP related photonic structures are shown to display quite isotropic photonic band gaps,[10] which are determined by the average interplane distance of the quasilattice.[11] It is reported that localized states exist inside the photonic gap in dodecagonal (12-fold symmetry) structures.[12] The reason for the localization is attributed essentially to the locally high density of dielectric scatterers on the maximum symmetry (12-fold) local centers. The same study suggests, however, that localization is not a general phenomenon in 2D high-symmetry QP structures since it concludes that there is no localization in QP structures with lower than 12-fold rotational symmetry order, namely the decagonal (10-fold) and octagonal (8-fold) structures, although they both contain maximum symmetry (respectively 10- and 8-fold) local centers.[12] On the contrary, a more recent investigation shows that gap edge related lasering effect involves localization in k space in QP photonic structures of decagonal symmetry.[13] For comparison, we can mention an early study on a model atomic decagonal AlMn alloy, where a strong tendency toward the localization is found for certain atomic vibrational states,[14] resulting from the coupling between vibrational modes propagating along and perpendicularly to the quasiperiodic atomic plane. As a matter of fact, the 1D dielectric Fibonacci sequence reflects only the lack of periodicity, but not the high degree symmetry of the quasilattice. In the case of 2D dielectric structures, it is unclear how the electromagnetic modes are affected by the global QP order or the symmetry order of the local lattice patterns, and the underlying mechanisms remain unknown as well. Further, structure disorders are known to lead to localization in classic structures; it is interesting to investigate their effects in the QP structures.

In this work, we consider the octagonal QP dielectric structure, which is both simple and representative of QP structures containing maximum symmetry local centers, and results can be generalized to those QP cases. We will study local structure effects and show that light wave modes at the photonic gap edges are localized on certain particular local structures that characterize both the QP and approximant structures, and we propose an explanation in a framework similar to the molecular orbital (MO) theory. The QP lattice and its approximants are intimately related. Indeed, a QP lattice can be successively approached by its approximants of increasing size. The latter are, moreover, of particular interest if we are interested in local structure effects, since they contain the same local patterns as the former. And, thanks to their periodicity, exact solution of Maxwell's equations can be obtained. The octagonal QP lattice is defined by the cut-and-projection algorithm used previously.[11] It can be approached through the same method by its best approximants of order $p_n/q_n = 1/1, 3/2, 7/5, \ldots$, which approximates the irrational number $\sqrt{2}$.[11] There are six local patterns in an octagonal QP lattice, among which is the maximum symmetry (8-fold) local center (the octagonal pattern A), as shown in Fig. 1(a). The 3/2 approximant is the lowest order (thus the simplest) best approximant structure that contains all of them (see the same figure). It is therefore a good candidate for investigating local structure effects.

The approximant dielectric structure is formed by scatter-

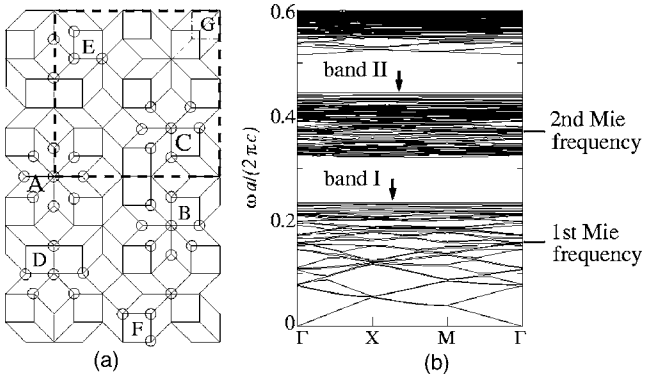

FIG. 1. (a) A portion of the 3/2 approximant of the octagonal quasilattice, formed by square and 45° rhombus tiles. The unit cell is bordered by dashed lines. The six local patterns characterizing the quasilattice are marked by circles and labeled from A to F. G shows a tile flip without lattice distortion. (b) The band diagram of the 3/2 approximant calculated for the TM polarization. The frequency levels of the first two Mie resonances are also indicated.

ers that are infinite high dielectric cylinders of $\epsilon=13$ and radius $r=0.28a$, with a the tile edge length. The cylinders are placed perpendicular to the lattice plane at the lattice nodes in an air background. Maxwell's equations are solved for TM polarization using a plane-wave method. The obtained band diagram is shown in Fig. 1(b), which displays two main photonic gaps similar to that obtained in Ref. 11. The bands below the two main photonic gaps [at, respectively, $\bar{\omega}=0.24$ and $\bar{\omega}=0.45$ $(\omega a/2\pi c)$], which will be referred as I and II in the following, display a strong flatness $(\Delta\bar{\omega}/\bar{\omega}<10^{-3}$ and $<10^{-4}$, respectively), implying a strong group speed reduction for the whole bands (see below). The electric field patterns corresponding to bands I and II are displayed in Fig. 2. This figure shows clearly that for both bands, the electric field is localized on the same octagonal ring of pattern A in Fig. 1(a), which is the most symmetrical local pattern. For band I, the electric field forms octapole modes

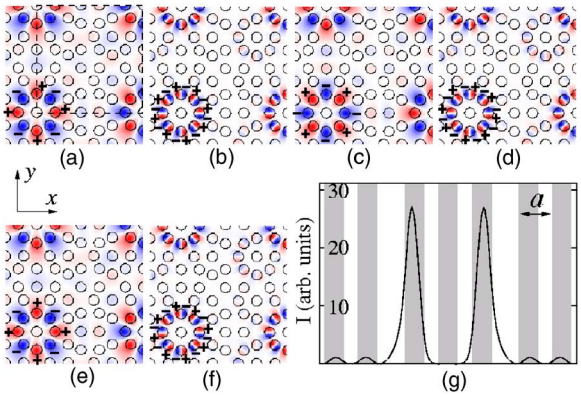

FIG. 2. (Color online) Electric-field patterns at Γ, X, and M points for bands I [(a), (c), and (e)] and II [(b), (d), and (f)] in the 3/2 octagonal approximant. The "+" and "–" signs indicate the field polarities. The unit cell is bordered by dashed lines. The field intensity in a slice passing through the ring center along the x axis is displayed in (g), where the shadowed zones represent the cross sections of the cylindrical scatterers.

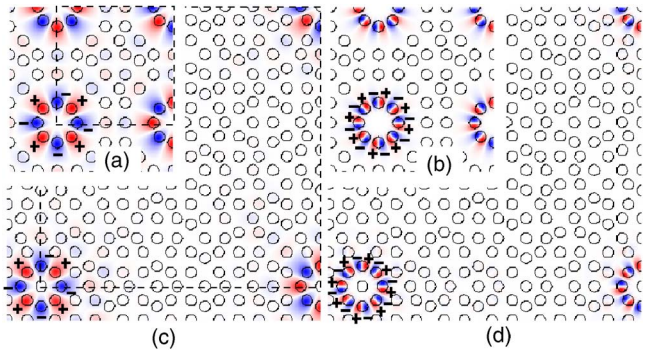

FIG. 3. (Color online) (a,b) Electric-field patterns for bands I and II in the 3/2 approximant, where the adjacent scatterers inside and outside of the octagonal ring are removed. (c,d) Field patterns in a tile-flipped 7/5 approximant containing only one octagonal ring per cell. The "+" and "–" signs indicate the field polarities.

while for band II it forms hexadecapole ones. The field intensity on the octapole, normalized to unity on an area of a^2, is displayed in the same figure in a slice along the x direction. It shows well that the intensity is essentially confined on the ring. The intensity follows a Gaussian-like distribution on each cylinder, with a peak width that corresponds roughly to the cylinder diameter.

The intensity distribution in Fig. 2 suggests that the field patterns are essentially determined by the scatterers on the octagonal ring, and that the adjacent structures are not significantly concerned. This suggests a local interaction mechanism. To investigate this, we first remove the adjacent cylinders both inside and outside the ring. We find that the corresponding band frequencies, as well as the electric-field patterns [Figs. 3(a) and 3(b)], remain unchanged. This indicates that the multipole mode formation is dominated by the nearest-neighbor interaction. Indeed, the octagonal quasilattice displays two internode distances, namely a and $(\sqrt{2-\sqrt{2}})a$ $(\approx 0.77a)$. The nodes on the ring are separated by the shorter one. Moreover, we can increase the interring distance by considering the 7/5 approximant that contains seven rings per cell. We introduce tile flips [as exemplified by G in Fig. 1(a)] in the cell so that only one ring per cell remains, and the interring distance is increased to $(7+5\sqrt{2})a$. We can check that the same multipole modes are formed on the rings [see Figs. 3(c) and 3(d)], with the same mode frequencies as the 3/2 approximant. This shows that these modes are independent of interring distance and are not caused by interring interference.

The above analyses indicate that the localized modes result essentially from nearest-neighbor coupling on high-symmetry local patterns. In order to investigate this phenomenon, let us consider an individual ring with the same physical and geometrical parameters. An octagonal ring is described by the D_8 group, of which the character table is given in Table I. We will consider here, in a framework similar to the MO theory, the s and the tangential p (denoted as p_T) waves on the cylinders. The characters of their respective representations, namely Γ_S and Γ_T, are given in the same table.

Under the D_8 group, Γ_S and Γ_T can be decomposed into

TABLE I. The character table of the D_8 group. The characters of the Γ_S and Γ_T representations are also listed.

D_8	E	$2C_8$	$2C_4$	$2C_8^3$	C_2	$4C_2'$	$4C_2''$
$\Gamma_1(A_1)$	1	1	1	1	1	1	1
$\Gamma_2(A_2)$	1	1	1	1	1	−1	−1
$\Gamma_3(B_1)$	1	−1	1	−1	1	1	−1
$\Gamma_4(B_2)$	1	−1	1	−1	1	−1	1
$\Gamma_5(E_1)$	2	$\sqrt{2}$	0	$-\sqrt{2}$	−2	0	0
$\Gamma_6(E_2)$	2	0	−2	0	2	0	0
$\Gamma_7(E_3)$	2	$-\sqrt{2}$	0	$\sqrt{2}$	−2	0	0
Γ_S	8	0	0	0	0	2	0
Γ_T	8	0	0	0	0	−2	0

$$\Gamma_S = \Gamma_1 + \Gamma_3 + \Gamma_5 + \Gamma_6 + \Gamma_7, \tag{1}$$

$$\Gamma_T = \Gamma_2 + \Gamma_4 + \Gamma_5 + \Gamma_6 + \Gamma_7, \tag{2}$$

where Γ_1 and Γ_3 describe, respectively, the bonding and the antibonding states of the s wave; Γ_2 and Γ_4 those of the p_T wave; and Γ_5, Γ_6, and Γ_7 the partially bonding, the nonbonding, and the partially antibonding states of both waves. The last three states are all doubly degenerate.

Indeed, the field patterns of bands I and II are described, respectively, by Γ_3 and Γ_4 representations. We will show in the following that they can effectively be considered as the antibonding states of, respectively, the s and p_T waves on the ring. We first compute the eigenmodes of the octagonal ring. To achieve this, we put the octagonal ring at the center of a cylindrical cavity in a dielectric medium, in which additional holes can be placed. Maxwell's equations are solved using a periodic square boundary condition. The parameters of the structure surrounding the ring (dielectric constant, hole size, and interhole distance) can be modulated to reduce complications arising from the coupling with the wave modes resulting from the imposed boundary condition, and to check that the obtained eigenfrequencies on the octagonal ring are not artifacts due to the surrounding structure.

Actually, all the field patterns described by the representations in Eqs. (1) and (2) are obtained (Fig. 4). The corresponding frequencies are listed in Table II, where $\bar{\omega}/\bar{\omega}'$ denotes the slight frequency shifts following the lift of the double degeneracy of the Γ_6 states, due to the imposed

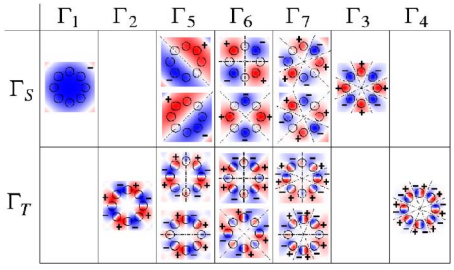

FIG. 4. (Color online) Electric-field patterns of the s and p_T eigenmodes on the octagonal ring. The "+" and "−" signs indicate the field polarities.

TABLE II. The eigenfrequencies of the s and p_T modes on the octagonal ring.

	Γ_1	Γ_2	Γ_5	Γ_6	Γ_7	Γ_3	Γ_4
Γ_S	0.10		0.12	0.17/0.18	0.22	0.24	
Γ_T		0.34	0.36	0.39/0.40	0.43		0.45

square boundary condition. We note, in particular, that $\bar{\omega}_{\Gamma_3}$ and $\bar{\omega}_{\Gamma_4}$ correspond, respectively, to the frequency levels of bands I and II.

In the nearest-neighbor approximation, the interscatterer interaction is described by a coupling parameter g that is proportional to $\langle \phi_n^* | H | \phi_{n+1} \rangle$, with $|\phi_n\rangle$ the wave function on the nth scatterer and H the Hamiltonian. The energy levels can easily be calculated using Hückel theory.[15] For a weak g value, we obtain the frequency levels

$$\omega = \omega_0 + g, \omega_0 + g/\sqrt{2}, \omega_0, \omega_0 - g/\sqrt{2}, \omega_0 - g \tag{3}$$

for an octagonal ring, where ω_0 stands for the mode frequency on an isolated individual scatterer. These frequency levels correspond, respectively, to those of Γ_1 (Γ_2), Γ_5, Γ_6, Γ_7, and Γ_3 (Γ_4) states. Equation (3) implies that the frequency differences between Γ_i ($i=1,\ldots,7$) and the nonbonding states (Γ_6), $\Delta\bar{\omega}_{\Gamma_i} = \bar{\omega}_{\Gamma_i} - \bar{\omega}_{\Gamma_6}$, are symmetrical for $i=(5,7)$ and $(1,3)$ and $(2,4)$, and that the frequency difference ratio $\Delta\bar{\omega}_{\Gamma_i}/\Delta\bar{\omega}_{\Gamma_j} = \sqrt{2}$ for $(i,j)=(3,7)$, $(1,5)$, $(4,7)$, and $(2,5)$. The values in Table II follow closely these relations.

In order to understand the origin of the local mode formation, let us consider the nonbonding states (Γ_6). Indeed, their frequencies can be related to the first two Mie resonances,[16] which occur for an infinite cylinder of $\epsilon=13$ for the size parameter $x=2\pi r/\lambda=0.29$ and 0.65, with λ the incident wave length. This corresponds to the frequencies $\bar{\omega}=0.16$ and $0.37(\omega a/2\pi c)$. These two frequencies are very close to $\bar{\omega}_{\Gamma_6}$ for, respectively, the s and p_T waves (Table II), and the slight differences can be explained if we consider that individual Mie states decay slowly (asymptotically as $1/r$) and residual interaction between next-neighbor cylinders can subsists.

The above analyses show that the field patterns as well as the frequency levels of bands I and II are indeed determined by the local ring patterns alone. The field distribution can be considered, moreover, as, respectively, the s and p_T antibonding states of the first two Mie resonance modes in a tight-binding framework. It is worth noting that here the Mie frequencies lie far from the gaps [see Fig. 1(b)], contrary to the simple periodic cases, where the Mie resonances are found directly related to the gap opening.[17]

The fact that the highest symmetry patterns yield the highest frequency modes is not surprising, if we consider that these patterns imply the strongest nearest-neighbor number, and thus the highest frequencies for the antibonding states. Local patterns with fewer nearest neighbors will form antibonding states with lower frequencies. As an example, pattern B of Fig. 1(a) contains seven nearest-neighbor scatterers, and leads to the antibonding states displayed in Fig. 5,

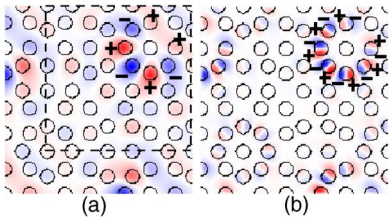

FIG. 5. (Color online) Electric-field patterns corresponding to the next frequency levels below, respectively, bands I (a) and II (b). The "+" and "−" signs indicate the field polarities. These modes are formed on pattern B in Fig. 1(a).

which correspond to frequency levels lying just below bands I and II. This illustrates also the reason why bands I and II do not lie deep in the main gaps, but rather at the low edges, since various patterns lead to different modes (with, of course, possible coupling between them as well as with extended modes) with frequency levels below these two bands. Such localization effects should be a common phenomenon for QP and approximant structures that are characterized by maximum symmetry local patterns.

Another point of interest is the effect of disorder in such systems. To investigate this, we introduce structure disorders by randomly flipping the tiles in the 3/2 approximant lattice in the way exemplified by G in Fig. 1(a). The resulting structures are randomly tiled, though neither node density modification nor lattice distortion are involved. Maxwell's equations are solved on the resulting structures. The obtained band diagrams are similar to that of the perfect structure in Fig. 1. The field distributions, however, are strongly modified. Figure 6 shows two examples [(a) and (b)], where the electric-field distributions are obviously more extended, and we can thus expect a better light propagation. Indeed, as shown in Fig. 6(f) (curves *a* and *b*), strong increases of the light group velocities (v_g), which can reach one magnitude as compared to that for the perfect structure (curve *p*), are obtained. This behavior contrasts with the classical cases where structure disorders are known to lead to localization effects. In the present case, however, this can be understood if we consider that the low group velocity in the perfect structure is related to the localization that occurs on the octagonal rings. Disorders decrease local symmetry order, implying lower numbers of nearest-neighbor scatterers, and thus disfavor the formation of localized high-frequency antibonding states, leading to group velocity increase. This is again characteristic of QP structures of $D \geq 2$, where structure disorders break the local symmetry of perfect lattices. We can also alter the structure order through local rearrangements in specific regions, by introducing disorders only in the regions surrounding pattern A [Fig. 6(c)], or by transforming pattern A into a square while taking care not to generate a new octagon [Fig. 6(d)]. It is worth noting that in the latter case the replacement of the octagon by the square, achieved by four tile flips, is a local order violation, since a perfect QP lattice does not contain such square patterns formed by four square tiles [see the six local patterns in Fig. 1(a)]. So the structure in Fig. 6(d) is an approximant structure containing locally defects that decrease the symmetry order of pattern A. The corresponding group velocities for these two structures

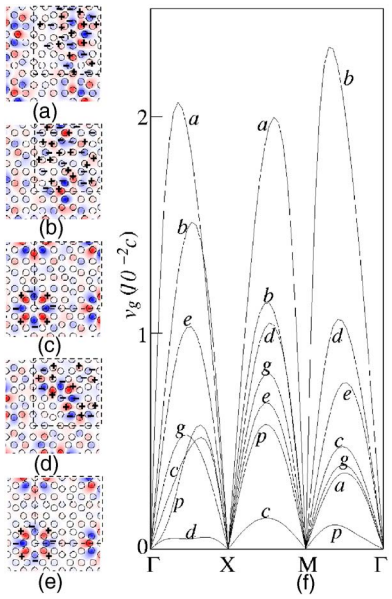

FIG. 6. (Color online) Electric-field patterns of band I in structures following various rearrangements, where the "+" and "−" signs indicate the field polarities: (a) and (b) the structures are randomized; (c) disorders are introduced only in regions surrounding pattern A; (d) the octagonal ring in pattern A is transformed into a square; (e) the octagonal symmetry of pattern A is broken. The corresponding group velocities are labeled from *a* to *e* and displayed in (f), where curves *p* and *g* are group velocities of, respectively, band I and the band next to it in the perfect structure of Fig. 1(a).

are displayed in Fig. 6(f) as well. The $v_g$curves (*c* and *d*) show that these modifications lead to anisotropic v_g changes following different directions. In particular, v_g is significantly increased in two out of three directions in the case of (d). This confirms that the low group velocity is essentially related to the antibonding states on the octagonal rings. Besides, structure modulation in surrounding regions affects interring correlation.

Generally, highly symmetrical local patterns in dielectric structures imply high local scatterer densities, but the latter do not necessarily mean the former. Indeed, for perfect QP structures characterized by high-symmetry local patterns, the symmetrical distribution of scatterers in the local patterns plays an important role in the localization process. Figure 6(e) provides an illustration where we introduce distortion in pattern A by slightly shifting (for ≤20% of the interscatterer distance) some scatterers on the octagonal ring from their initial positions, so that the local octagonal symmetry is broken, but all eight scatterers remain on the ring and the density of pattern A is unchanged. As shown by the same figure, the corresponding field distribution on the octagonal ring varies following the scatterers. The group velocity [curve *e* in Fig. 6(f)] is significantly increased in all three directions as compared to curve *p*. As a matter of fact, this can also be understood in the framework of nearest-neighbor resonances, since asymmetrical scatterer distribution leads to dispersion in the coupling between neighbor scatterers, resulting in less flat frequency dispersion curve. Indeed, the width of band I resulting from the above structure distortion is twice as large

in frequency as compared to the perfect structure.

Finally, we note that there are numerous bands in the two frequency ranges below, respectively, bands I and II. Some of them correspond to localized states as well but on different local structure patterns. And they are all less flat than, respectively, bands I and II. For example, as mentioned above, the band lying just below band I corresponds to the mode on pattern B [Fig. 5(a)]. This band is the second flattest next to band I in the corresponding frequency range. The corresponding group velocity [curve *g* in Fig. 6(f)] is globally higher than that of band I (curve *p*).

The present work differs from Ref. 12, by showing that localization occurs in QC structures due to nearest-neighbor resonances, and that symmetry distribution of scatterers in local patterns, rather than their density, constitutes the most favorable localization condition. Moreover, we show that localization does occur in lower-order rotational symmetry QP structures, thus suggesting that this can indeed be a general phenomenon for QP structures containing maximum symmetry local centers. It is also worth mentioning that the transport behavior in an infinite-sized QP system can be more complicated as compared to approximants of finite-sized unit cells. However, the results of the present work can still qualitatively hold, since all the characteristic local patterns of the parent QP lattice are contained in the approximants, and the unit cells of the latter are repeated infinitely many times in the QP lattice. Moreover, in practice, QP samples of finite size can be considered as equivalent to approximants.

In summary, we studied the light wave states in quasiperiodic dielectric media through investigations on the approximant structures. We have shown that the bands below the main photonic gaps are formed by states localized on the highest symmetry local patterns that are common to the quasilattice and the approximants. Unlike the classical localization case, here the localized states are not related to destructive interference, but rather determined by resonances between local nearest-neighbor scatterers at Mie resonance modes. More particularly, structure disorders can lead to more extended field distribution and strong increase in light propagation. This study can trigger direct experimental observations, such as light wave distribution and transmission in high-symmetry quasiperiodic and related dielectric structures in the localization regime. It also provides a new physical mechanism of optical confinement and light slowing. The same approach can be generalized to other 2D and 3D quasiperiodic structures, as well as to other wave cases such as sound propagation.

*Electronic address: wang@lps.u-psud.fr

[1] P. W. Anderson, Phys. Rev. **109**, 1492 (1958).
[2] S. John, Phys. Rev. Lett. **53**, 2169 (1984); A. Z. Genack and N. Garcia, *ibid.* **66**, 2064 (1991); D. S. Wiersma, P. Bartolini, Ad. Lagendijk, and R. Righini, Nature (London) **390**, 671 (1997).
[3] See, for example, *Photonic Crystals and Light Localization in the 21st Century*, edited by C. M. Soukoulis (Kluwer Academic Publishers, Dordrecht, 2001), and references therein.
[4] S. John, Phys. Rev. Lett. **58**, 2486 (1987).
[5] E. Yablonovitch, Phys. Rev. Lett. **58**, 2059 (1987).
[6] M. Kohmoto, B. Sutherland, and K. Iguchi, Phys. Rev. Lett. **58**, 2436 (1987).
[7] E. Maciá, Phys. Rev. B **63**, 205421 (2001).
[8] R. W. Peng, Y. M. Liu, X. Q. Huang, F. Qiu, Mu Wang, A. Hu, S. S. Jiang, D. Feng, L. Z. Ouyang, and J. Zou, Phys. Rev. B **69**, 165109 (2004).
[9] L. Dal Negro, C. J. Oton, Z. Gaburro, L. Pavesi, P. Johnson, Ad. Lagendijk, R. Righini, M. Colocci, and D. S. Wiersma, Phys. Rev. Lett. **90**, 055501 (2003).
[10] Y. S. Chan, C. T. Chan, and Z. Y. Liu, Phys. Rev. Lett. **80**, 956 (1998); S. David, A. Chelnokov, and J. M. Lourtioz, Opt. Lett. **25**, 1001 (2000).
[11] K. Wang, S. David, A. Chelnokov, and J. M. Lourtioz, J. Mod. Opt. **50**, 2095 (2003).
[12] Y. Wang, X. Hu, X. Xu, B. Cheng, and D. Zhang, Phys. Rev. B **68**, 165106 (2003).
[13] M. Notomi, H. Suzuki, T. Tamamura, and K. Edagawa, Phys. Rev. Lett. **92**, 123906 (2004).
[14] J. Hafner, M. Krajčí, and M. Mihalkovic, Phys. Rev. Lett. **76**, 2738 (1996).
[15] See R. G. Parr, *Quantum Theory of Molecular Electronic Structure* (Benjamin, New York, 1963), Chap. III.
[16] See C. F. Bohren and D. R. Huffman, *Absorption and Scattering of Light by Small Particles* (Wiley, New York, 1983), Chap. 4 and Appendix C.
[17] Z. Zhang and S. Satpathy, Phys. Rev. Lett. **65**, 2650 (1990).